Interference Prediction in Wireless Networks: Stochastic Geometry Meets Recursive Filtering

Jorge F. Schmidt, Udo Schilcher, Mahin K. Atiq, and Christian Bettstetter, *Senior Member, IEEE*

***Abstract*—This article proposes and evaluates a technique to predict the level of interference in wireless networks. We design a recursive predictor that estimates future interference values by filtering measured interference at a given location. The predictor's parameterization is done offline by translating the autocorrelation of interference into an autoregressive moving average (ARMA) representation. This ARMA model is inserted into a steady-state Kalman filter enabling nodes to predict with low computational effort. Results show a good accuracy of predicted values versus true values for relevant time horizons. Although the predictor is parameterized for Poisson-distributed nodes, Rayleigh fading, and fixed message lengths, a sensitivity analysis shows that it also tends to work well in more general network scenarios. Numerical examples for underlay device-to-device communications, a common wireless sensor technology, and coexistence scenarios of Wi-Fi and LTE illustrate its broad applicability. The predictor can be applied as part of interference management to improve medium access, scheduling, and radio resource allocation.**

***Index Terms*—Wireless systems, interference, prediction, stochastic geometry, ARMA, Kalman filter.**

I. Introduction

THE management of interference has always been a key issue in wireless systems [1]. Negative effects of interference are averted by radio resource management, medium access control, scheduling, and decoding techniques. Positive aspects may include physical-layer security and energy harvesting from radio waves. In all cases, it seems beneficial to have the ability to *predict* interference into the future — an approach that has not been investigated comprehensively and for which a technique is proposed and evaluated in this article.

Interference can be modeled as a random variable whose properties depend on several parameters, including node locations, mobility, and data traffic. Some properties — including mean interference, higher-order statistics, and distributions — can be calculated in a given setup using stochastic geometry [2]–[8]. These results consider the spatial features of wireless networks, which makes them fundamentally different from "classical" pieces of work on interference modeling and analysis [9], [10]. A branch of research analyzes how interference *changes* over time and space [11]–[17]. Such interference dynamics can be expressed in terms of the autocorrelation of the received interference. Correlation influences the system behavior, such as the performance of diversity, relaying, multiple-input multiple-output (MIMO), and medium access protocols (see [13], [14], [18], [19]).

Despite advances in the modeling of interference dynamics, this knowledge has not been exploited to actually improve the performance of wireless systems [20]. The state of research is not as advanced as in channel modeling, where insights on channel dynamics — such as coherence time and decorrelation distances — are indeed used in practice (e.g., space-time coding and MIMO). Taking this step from modeling to design is the goal of our research: the investigation of interference prediction. The fundamental question at the core of our work is: "How well can one predict, in a probabilistic manner, the interference power at a given location in a certain network?" Initial steps in this direction were made in [20], which proposes a simple prediction technique based on learning of traffic patterns, and by others in [21], which proposes prediction based on the mobility of nodes without considering traffic and channel. Furthermore, contention-based medium access control protocols perform some type of *implicit* estimation of future interference levels through their inherent (exponential) backoff techniques.

Our approach for predicting the level of interference is to merge results on the autocorrelation of interference [17] with recursive filtering. The specific contributions are as follows:

1) A method is presented to map the autocorrelation function of interference into an autoregressive moving average (ARMA) model suited for performing forecasts from previous interference observations. This mapping is calculated for Poisson distributed nodes, Rayleigh fading, and random medium access with fixed message lengths.
2) An offline and blind predictor is obtained by inserting the ARMA representation of the interference process into a

Manuscript received October 1, 2020; revised December 30, 2020; accepted February 1, 2021. Date of publication February 12, 2021; date of current version April 2, 2021. This work was supported in part by the Austrian Science Fund (FWF) under Grant P24480-N15 (Dynamics of interference in wireless networks) and in part by the K-project DeSSnet (Dependable, secure and time-aware sensor networks). The project DeSSnet is funded within the context of COMET Competence Centers for Excellent Technologies by the Austrian Federal Ministry for Climate Action, Environment, Energy, Mobility, Innovation (BMK), the Federal Ministry for Digital and Economic Affairs (BMDW), and the federal states of Styria and Carinthia; the COMET program is conducted by theAustrian Research Promotion Agency (FFG). The review of this article was coordinated by Dr. C. Yuen. *(Corresponding author: Udo Schilcher.)*

Jorge F. Schmidt is with the Institute of Networked and Embedded Systems, University of Klagenfurt, Lakeside Park B02, Klagenfurt 9020, Austria, and also with Lakeside Labs GmbH, Lakeside Park B04, Klagenfurt 9020, Austria (e-mail: Jorge.Schmidt@aau.at).

Udo Schilcher and Christian Bettstetter are with the Institute of Networked and Embedded Systems, University of Klagenfurt, Lakeside Park B02, Klagenfurt 9020, Austria (e-mail: udo.schilcher@aau.at; christian.bettstetter.@aau.at).

Mahin K. Atiq was with the Institute of Networked and Embedded Systems, University of Klagenfurt, Klagenfurt 9020, Austria. She is now with Silicon Austria Labs GmbH, Graz 8010, Austria (e-mail: mahin.atiq@silicon-austria.com).

Digital Object Identifier 10.1109/TVT.2021.3059032

This work is licensed under a Creative Commons Attribution 4.0 License. For more information, see https://creativecommons.org/licenses/by/4.0/

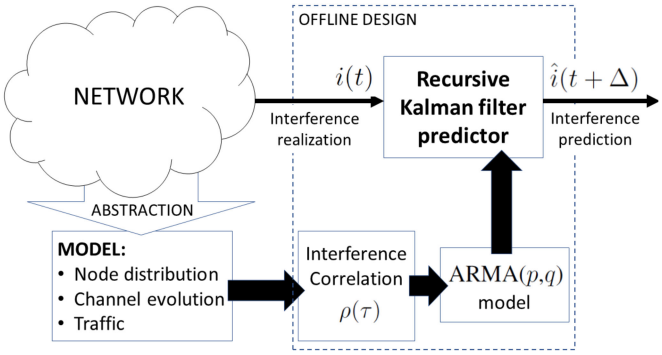

Fig. 1. Block diagram of the interference predictor.

Kalman filter. The time invariance of the model leads to a steady-state gain of the Kalman predictor to perform lightweight predictions at individual nodes. A block diagram of the predictor design is given in Fig. 1.

3) Simulations show that this predictor outperforms both basic predictors and predictors that consider only the channel dynamics (and disregard the impact of traffic).
4) A sensitivity analysis demonstrates the robustness of the predictor against certain inaccuracies and model mismatches in its parameterization: it performs well with traffic and node distribution models that are more general than the ones used in its design. Numerical examples for underlay device-to-device communications, a wireless sensor network, and coexistence scenarios of Wi-Fi and LTE illustrate the applicability of the proposed scheme.

The rest of the article is organized as follows. Section II introduces the system model. Section III derives the interference predictor, starting with the stochastic geometry models of interference and progressing to the low-complexity recursive predictor implementation. Section IV evaluates the predictor in terms of accuracy and includes a sensitivity analysis and specific technology examples. Finally, Section V concludes.

II. System Model

The system is described by the placement and mobility of nodes, their data traffic behavior, and the radio channel. Time is discretized into slots $t \in \mathbb{N}_0$. The parameterization of the predictor is done for the following *base system*.

Node positions follow a two-dimensional Poisson point process (PPP) $\Phi = \Phi(t)$ of intensity λ. All nodes move with speed ν following a time-discrete Brownian motion. This mobility model is chosen because it preserves the uniform spatial distribution: the node locations at a given time t form a PPP $\Phi(t)$ with intensity λ [22]. Other models with this property could also be applied. The location x of a node at time $t+\tau$ is $x_{t+\tau} = x_t + \nu\omega_\tau$, with $\omega_\tau = \sum_{t=1}^{\tau} \omega_t \stackrel{d}{=} \sqrt{\tau}\omega_0$, where the last equal sign denotes equality in distribution and the ω_t are i.i.d. two-dimensional Gaussian random variables of zero mean and covariance matrix

$$\Sigma = \begin{pmatrix} 0 & \sqrt{2/\pi} \\ \sqrt{2/\pi} & 0 \end{pmatrix}. \tag{1}$$

At a given slot t, each node is either idle or transmitting with power κ such that, on average, a fraction μ of all nodes starts a new transmission. The message duration ℓ is the same for all transmissions. In any slot, each idle node starts a transmission with probability $\frac{\mu}{1-\mu(1-\ell)}$. This yields an expected traffic intensity of $\mu\ell$ interferers in each slot [17]. Such a combination of node placement and random access is often used to model wireless sensor networks and (with some considerations) cellular networks, in particular for device-to-device communications (see [23]–[28]).

The channel is described by a standard model with distance-dependent attenuation and small-scale fading due to multipath propagation. The path gain is $g(x,\xi) = \min(1, \|x-\xi\|^{-\alpha})$ with path loss exponent $\alpha > 2$ and some normalization. Small-scale fading is modeled by Rayleigh fading with $\mathbb{E}[h^2(t)] = 1$. The channel gain $h^2(t)$ is then exponentially distributed. The Jakes-Doppler model [29] describes the continuous time evolution of the wireless channel. It assumes uniform scatterers' directions which makes it fit well for a wide range of propagation environments. Its amplitude's autocorrelation function is $\rho_J(\tau) = J_0(2\pi\tau\nu_{\max})$, where $J_0(\cdot)$ is the zeroth-order Bessel function of the first kind and $\nu_{\max} = \nu$ is the maximum expected speed. The channel coherence time η is the time lag for which the channel autocorrelation first reaches a small threshold, which is zero in this article.

A message transmitted at location x causes interference at ξ with power $i_{\xi_x}(t) = \kappa\, g(x,\xi)\, h_x^2(t)$. The overall interference at location ξ at time t is the sum of the reception powers from all transmitting nodes. In Poisson networks, the consideration of a typical location ξ is equal to the consideration at the origin of the plane $\mathbb{R}^2$ due to Slivnyak's theorem [30], [31]. In the given base system, the overall interference power is thus

$$i(t) = \sum_{x\in\Phi} i_{\xi_x}(t)\gamma_x(t) = \sum_{x\in\Phi} \kappa\, \min(1, \|x\|^{-\alpha})\, h_x^2(t)\, \gamma_x(t)\,, \tag{2}$$

where $\gamma(t)$ is a Bernoulli random variable indicating whether node x is sending ($\gamma_x(t) = 1$) or not ($\gamma_x(t) = 0$), condensing the information from the parameters μ and ℓ. The interference process in (2) is stationary [31] and changes over time due to the time-varying characteristics of node locations, wireless channel, and traffic. These sources of time-varying behavior are captured by the parameters ν, η, μ, and ℓ.

III. Interference Prediction

A. Interference Correlation

A main approach for channel prediction is based on exploiting the autocorrelation of the channel [32]. We take a similar approach for interference prediction: our design starts with an analytical model for the autocorrelation associated to the interference process. We use Pearson's correlation coefficient of $i(t)$ for two time instants t_1 and t_2, which is:

$$\rho(i(t_1), i(t_2)) = \frac{\mathrm{cov}[i(t_1), i(t_2)]}{\sigma_i^2}\,, \tag{3}$$

TABLE I
SYSTEM MODEL PARAMETERS

Setup	Speed ν	Traffic parameter μ	Message length ℓ	Channel coherence time η
1	0.77 cm/slot	0.01 / slot	10 slots	50 slots
2	1.91 cm/slot	0.01 / slot	10 slots	20 slots
3	7.65 cm/slot	0.01 / slot	10 slots	5 slots

where $\mathrm{cov}[i(t_1), i(t_2)] = \mathbb{E}[i(t_1)i(t_2)] - \mathbb{E}[i(t_1)]\,\mathbb{E}[i(t_1)]$ is the covariance of i, σ_i^2 its variance, and $\mathbb{E}[i]$ the expected value. The lag is denoted by $\tau = t_2 - t_1$.

Expressions for this correlation are known for different system models [17]. The model that parameterizes our predictor corresponds to Case (2,2,2) in [17], for which

$$\rho(i(t_1), i(t_2)) = \frac{\left(J_0^2(2\pi\tau\nu_{\max}) + 1\right)\mathbb{E}[\gamma(t_1)\,\gamma(t_2)]}{2\mu\ell} \cdot \frac{(\alpha-1)\int_{\mathbb{R}^2} g(x)\mathbb{E}[g(x+\nu\omega_\tau)]\mathrm{d}x}{\alpha\pi}, \quad (4)$$

where stationarity implies $\rho(i(t_1), i(t_2)) = \rho(i(t_2 - t_1))$, which we denote $\rho(\tau)$. The integral can only be solved numerically in case of mobility. The traffic contribution is [17]

$$\mathbb{E}[\gamma(t_1)\,\gamma(t_2)] = \max\left(0, \mu\left(\ell - \tau\right)\right) + \frac{\mu^2}{1-\mu(\ell-1)} \sum_{i=0}^{\min(\tau-1,\ell-1)} \sum_{j=1}^{\min(\tau-i,\ell)} \sum_{k=0}^{\lfloor \frac{g}{\ell} \rfloor} \binom{g-k\ell+k}{k} \beta^{g-k\ell}(1-\beta)^k$$

with $g = \tau - i - j$, and $\beta = 1 - \mu/(1 - \mu(\ell - 1))$ being the probability of a node staying idle in a slot. From (4) and [17, Th.2], the interference correlation when the channel is the sole source of correlation yields $\rho(\tau) = J_0^2(2\pi\tau\nu_{\max})$.

Similar to the characterization of channels, one can define the interference coherence time τ_c to be the lag until the correlation of interference is smaller than a threshold θ [17], i.e., $\tau_c = \min\{\tau \in \mathbb{N} \mid \rho(\tau) \leq \theta\}$. In contrast to the channel coherence time, there are scenarios for which the interference correlation does not reach zero [17]. To account for this, we set $\theta = 0.25$ as the threshold, which is reached by all scenarios in this article. Table I shows three combinations of parameter values to be used to yield a high, a moderate, and a low correlation. The interference correlation for these setups is shown in Fig. 2. These setups are used to illustrate some design steps and assess the performance of the predictor.

Fig. 3 illustrates the impact of different correlation sources on the overall interference. The upper plot shows the interference resulting from time-varying traffic over a time-varying channel. The lower plot shows the interference if all nodes transmit all the time over the same time-varying channel. The differences are visible and underline the limitations of channel prediction in an interference-dominated system.

We design an interference predictor based on the Kalman filter that harnesses the knowledge of the correlation (4) and is practically feasible in a sense that nodes can implement it with limited computational resources and without additional signaling. The interference in (2) is a nonlinear function of the considered sources of temporal correlation. Nonlinear approaches, like the extended or unscented Kalman filter, would be a natural choice for deriving an interference predictor. However, aiming at a predictor for resource constrained devices, we leave the use of nonlinear filters for future work.

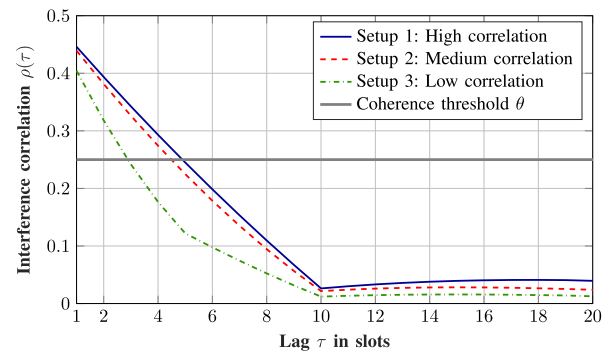

Fig. 2. Interference correlation for the setups of Table I. For a threshold $\theta = 0.25$, the interference coherence time is $\tau = 5$ slots (Setups 1 and 2) and $\tau = 3$ slots (Setup 3).

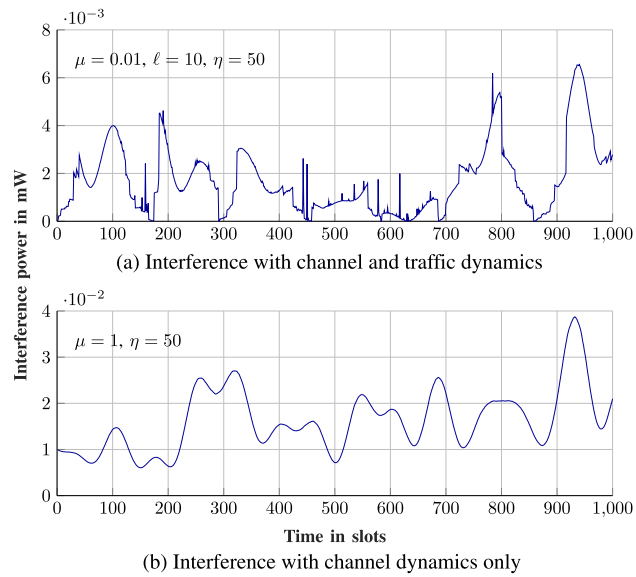

Fig. 3. Interference traces depicting the impact of traffic on the interference dynamics. Part (a) shows a realization of Setup 1 from Table I. Part (b) shows a realization of Setup 1 that ignores the traffic contribution ($\mu = 1$), only accounts for the channel dynamics. Transmit power $\kappa = 1$ mW.

B. ARMA Approximation of $\rho(\tau)$

ARMA models are extensively used in applications involving temporal stochastic processes. The Cramér-Wold theorem [33, Ch. 17] states that every stationary stochastic process has a moving average (MA) representation. If an autoregressive (AR) component is also used, the potential to accurately represent the process with a limited number of parameters greatly increases, making ARMA models particularly useful.

The ARMA representation of a process is typically identified from observing its realizations; the autocorrelation of the process is in general unknown. Such an identification approach requires several observations to identify the model dimension and its coefficients' values. These observations constitute a form of pilot signaling and can become impractically large in some

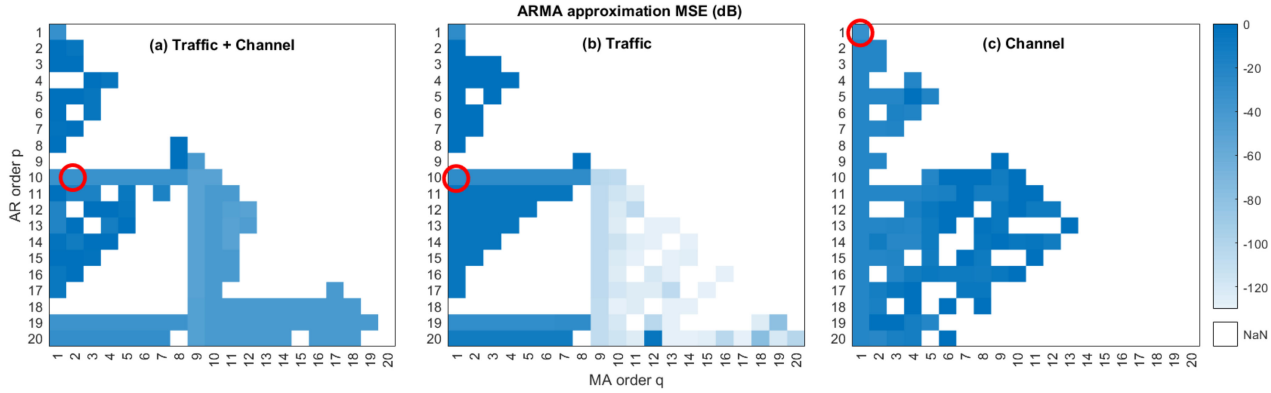

Fig. 4. Heatmaps showing the ARMA approximation MSE (dB) achieved by different (p, q)-pairs on three autocorrelation functions. Part (a) corresponds to Setup 1 from Table I, part (b) to Setup 1 simplified to have time-invariant channel conditions, and part (c) to the simplification of Setup 1 to have time invariant traffic. The selected model orders, meeting an MSE target of -30 dB, are highlighted with red circles.

cases, depending on the dynamics of the process to represent. Different to the typical case, we know $\rho(\tau)$ for a given system model in terms of the sources of correlation considered in (4). We are therefore interested in approximating it through an ARMA model with a small number of parameters.

The ARMA(p, q) representation of $i(t)$ can be written as

$$\sum_{n=0}^{p} a_n\, i(t-n) = \sum_{n=0}^{q} b_n\, \epsilon(t-n), \qquad q \leq p, \tag{5}$$

where the model orders p and q are in general unknown. The coefficients a_n and b_n specify the AR and MA components, respectively, and $\epsilon(t)$ is a zero-mean white noise. The model is normalized by setting $a_0 = b_0 = 1$.

The coefficients in (5) can be inferred from $\rho(\tau)$. Specifically, multiplying (5) by $i(t-\tau)$ and taking expectation yields

$$\sum_{n=0}^{p} a_n\, \rho(\tau - n) = \sum_{n=0}^{q} b_n \delta(n-\tau), \tag{6}$$

with the Dirac delta function $\delta(\cdot)$. Specializing for $\tau = q+1, \ldots, q+p$, the AR coefficients $a_1, \ldots, a_p$ can be found as the solution to the resulting Yule-Walker equations [34] (see Appendix A).

To determine the MA coefficients, an auxiliary sequence $\psi(t)$ defined to equal each side of (5) is introduced. Then:

$$\mathbb{E}[\psi(t)\, \psi(t-\tau)] := \sum_{m=0}^{p} \sum_{n=0}^{p} a_m\, a_n\, \rho(\tau+n-m) \tag{7}$$

$$= \sigma_\epsilon^2 \sum_{m=0}^{q} b_n\, b_{n+\tau}. \tag{8}$$

Since all terms on the right hand side of (7) are known, the terms $b_1, \ldots, b_q$ and σ_ϵ^2 can be solved for (see Appendix A) by equating that expression to (8).

Observe that in (6) and (7) only the first $p+q$ values of $\rho(\tau)$ are involved in the computation of the model coefficients. For a good representation, $p+q$ should be large enough to capture the main features of $\rho(\tau)$. If significant correlation exists for large τ-values, a decimation of $\rho(\tau)$ can be performed to reduce the number of significant lags prior to the parameter determination to keep $p+q$ low. A scaling down in frequency of the resulting ARMA model in the same decimation factor is then performed to bring the result to the same scale.

C. ARMA Model Order Selection

The described coefficient determination depends on the orders p and q and is thus not unique. Each (p, q)-pair results in an approximation error for $\rho(\tau)$; many pairs yield low errors, but not all pairs are suitable. The availability of $\rho(\tau)$ allows a least square approach to select the order values. Feasible (p, q)-pairs are those for which $\hat{\rho}_{p,q}(\tau) \to \rho(\tau)$ for $\tau \to \infty$. For this set and a largest significant correlation lag of T, the mean square approximation error is

$$\mathrm{MSE}(p, q) = \frac{1}{T} \sum_{\tau=1}^{T} \left(\rho(\tau) - \hat{\rho}_{p,q}(\tau)\right)^2. \tag{9}$$

Pair (p, q) is then chosen as that lowest order-p model meeting a target error. This selection criteria is illustrated in Fig. 4 for three different autocorrelation functions derived from Table I, considering $T = 100$ and a model order of up to $p = 20$. These examples show how the order is affected by the different sources of correlation.

To obtain the errors in Fig. 4, it is necessary to find the autocorrelation $\hat{\rho}_{p,q}(\tau)$ in (9) associated to a given (p, q)-pair, which we simply call $\hat{\rho}(\tau)$. Using $\hat{\rho}(\tau)$ in (6) and noting that $\delta(n-\tau) = \mathbb{E}[i(t-\tau)\epsilon(t-n)] = 0$ for $\tau > n$, it follows that

$$\sum_{n} a_n\, \hat{\rho}(\tau - n) = 0 \quad \text{for} \quad \tau > q. \tag{10}$$

Thus, knowing the $q+1$ nonzero values of $\delta(\cdot)$ and the p initial values of $\hat{\rho}(\cdot)$, (10) can be solved recursively for all values of $\hat{\rho}(\cdot)$ beyond p that are needed to compute (9).

To obtain the required nonzero δ-values, we follow [33, Ch. 17]. Multiplying (5) by $\epsilon(t-\tau)$ and taking expectation yields $\sum_{n=0}^{\tau} a_n\, \delta(\tau - n) = \sigma_\epsilon^2\, b_\tau$, which can be rearranged,

$$\delta_\tau = \frac{1}{a_0} \left(b_\tau \sigma_\epsilon^2 - \sum_{n=0}^{\tau} a_n \delta(\tau - n) \right), \tag{11}$$

to recursively find $\delta(0), \delta(1), \ldots, \delta(q)$. The p initial values of $\hat{\rho}(\cdot)$ are obtained by substituting $\delta(0), \delta(1), \ldots, \delta(q)$ and $\hat{\rho}(\cdot)$

in (6). Finally, the initial values of $\hat{\rho}(\cdot)$ are used to compute the succeeding ones using (10).

D. Recursive Interference Predictor

An interference predictor can be constructed from the ARMA(p, q) approximation of the interference process. Expressing the model coefficients as polynomials in the lag operator L and provided that the roots of the polynomial on a_n are outside the unit circle, the interference sequence becomes the filtered output of the noise sequence $\epsilon(t)$:

$$i(t) = \frac{b_0 + b_1\, L + \ldots + b_q L^q}{a_0 + a_1\, L + \ldots + a_p L^p}\, \epsilon(t). \tag{12}$$

This filter form suggests that it is possible to predict interference samples $\hat{i}(t+\Delta)$ by feeding (12) with a white noise sequence. However, such open loop prediction has poor accuracy given the sample autocorrelation dispersion between different realizations of the interference process. Nevertheless, a closed loop Kalman formulation of the filtering problem gives accurate predictions as will be shown in the next section.

For deriving the Kalman filter recursion, we first map our ARMA model into a state space form:

$$\mathbf{x}(t+1) = \mathbf{A}\mathbf{x}(t) + \mathbf{B}\epsilon(t) \tag{13}$$

$$i(t) = \mathbf{C}\mathbf{x}(t), \tag{14}$$

with state vector $\mathbf{x}$ of size $p \times 1$, transition matrix

$$\mathbf{A} = \begin{bmatrix} a_1 & a_2 & \cdots & a_{p-1} & a_p \\ 1 & 0 & \cdots & 0 & 0 \\ 0 & 1 & \cdots & 0 & 0 \\ \vdots & \vdots & \ddots & \vdots & \vdots \\ 0 & 0 & \cdots & 1 & 0 \end{bmatrix}, \tag{15}$$

and $\mathbf{B} = [1\ 0 \cdots 0]^{\mathrm{T}}$ and $\mathbf{C} = [0 \cdots 0\ b_0 \cdots b_q]$ of length p.

Assuming unitary process and measurement noise and following [35], the Kalman recursion for tracking $i(t)$ can be initialized with an all-zero state vector and an initial error covariance $\mathbf{P} = \mathbf{B}\mathbf{B}^{\mathrm{T}}$. At each iteration of the filter, the measurement update is

$$\mathbf{M} = \mathbf{P}\mathbf{C}^{\mathrm{T}} \left(\mathbf{C}\mathbf{P}\mathbf{C}^{\mathrm{T}} + 1\right)^{-1} \tag{16}$$

$$\mathbf{x}(t) = \mathbf{x}(t) + \mathbf{M}(i(t) - \mathbf{C}\mathbf{x}(t)) \tag{17}$$

$$\mathbf{P} = (\mathbf{I}_p - \mathbf{M}\mathbf{C})\mathbf{P}, \tag{18}$$

with the innovation gain $\mathbf{M}$ and identity matrix $\mathbf{I}_p$ of size p. The time update is

$$\mathbf{x}(t+1) = \mathbf{A}\mathbf{x}(t) + \mathbf{B}(i(t) - \mathbf{C}\mathbf{x}(t)) \tag{19}$$

$$\mathbf{P} = \mathbf{A}\mathbf{P}\mathbf{A}^{\mathrm{T}} + \mathbf{B}\mathbf{B}^{\mathrm{T}}. \tag{20}$$

As the interference process is time invariant and the model described by (12) and (13) is assumed to be reachable and detectable, the error covariance $\mathbf{P}$ converges to a constant [35], and (16) to (20) reduce to a steady-state Kalman filter of gain $\mathbf{K}$:

$$\mathbf{x}(t+1) = \mathbf{A}\mathbf{x}(t) + \mathbf{K}(i(t) - \mathbf{C}\mathbf{x}(t)). \tag{21}$$

The interference prediction for a prediction horizon Δ can finally be found by extrapolating the state vector Δ time slots into the future on each iteration and using (14):

$$\tilde{\mathbf{x}} = \mathbf{A}^{\Delta-1}\mathbf{x}(t+1), \qquad \hat{i}(t+\Delta) = \mathbf{C}\tilde{\mathbf{x}}. \tag{22}$$

The gain $\mathbf{K}$ can be computed offline, which reduces the online effort of the predictor to the state update in (21) and to the extrapolation of the filter through (22).

Let us summarize the steps with the block diagram in Fig. 1. From a network model abstraction, the interference autocorrelation is obtained from (4). This is used to parameterize an ARMA(p, q) model, which is inserted into a steady-state Kalman filter to complete the predictor's offline design. Predicted samples $\hat{i}(t+\Delta)$ are filtered samples of $i(t)$.

TABLE II
IMPLEMENTATION COST IN OPERATIONS REQUIRED

Type of operation	Standard predictor	Steady-state predictor
Measurement update	$2p^3 + 4p^2 + 9p$	–
Time update	$4p^3 + 2p^2 + 6p$	$p^2 + 3p$
Prediction	$2(\Delta - 2)p^3 + 2p^2 + 2p$	

E. Complexity Analysis

We quantify the implementation cost in terms of memory requirements and the number of sum and product operations needed to compute one predicted sample. These follow from (21) for the proposed steady-state Kalman recursion and from (16) to (20) for the standard Kalman predictor. The prediction step of (22) completes the analysis for both. The implementation cost of the standard Kalman recursion helps to assess the computational gains from the steady-state formulation.

1) Memory: For a model of order p, the standard Kalman filter stores the matrices $\mathbf{A}$ and $\mathbf{P}$, vectors $\mathbf{B}, \mathbf{C}, \mathbf{M}, \mathbf{x}$, and $\tilde{\mathbf{x}}$, and scalars $i(t)$ and $\hat{i}(t+\Delta)$, requiring $2p^2 + 5p + 2$ floating point memory units. The steady-state formulation requires storage for matrix $\mathbf{A}$, vectors $\mathbf{C}, \mathbf{K}, \mathbf{x}$, and $\tilde{\mathbf{x}}$, and scalars $i(t)$ and $\hat{i}(t+\Delta)$, amounting to $p^2 + 4p + 2$ memory units. For practical model orders (Fig. 4), both formulations have low and similar memory requirements.

2) Computations: We make some approximations that simplify analysis but still capture the main floating point operation costs. The vector-vector product is approximated to require $2p$ operations, the vector-matrix product $2p^2$ operations, and the matrix-matrix product $2p^3$ operations. Operations with scalars are disregarded. We distinguish between computations for the measurement and time updates, and for the prediction. We find that a standard Kalman predictor evaluates (16) to (18) for the measurement update, and (19) and (20) for the time update. In the case of the steady-state Kalman predictor, the measurement update is not evaluated since the steady-state gain $\mathbf{K}$ is computed offline. For the time update, (21) is evaluated. Finally, both predictors use (22) to obtain the predicted interference sample. Table II summarizes the computational costs.

Fig. 6 shows the advantage of the steady-state formulation in terms of complexity. The computational cost for a prediction horizon of $\Delta = 5$ using the steady-state predictor (dashed trace with marker) is lower than that of $\Delta = 2$ using the standard

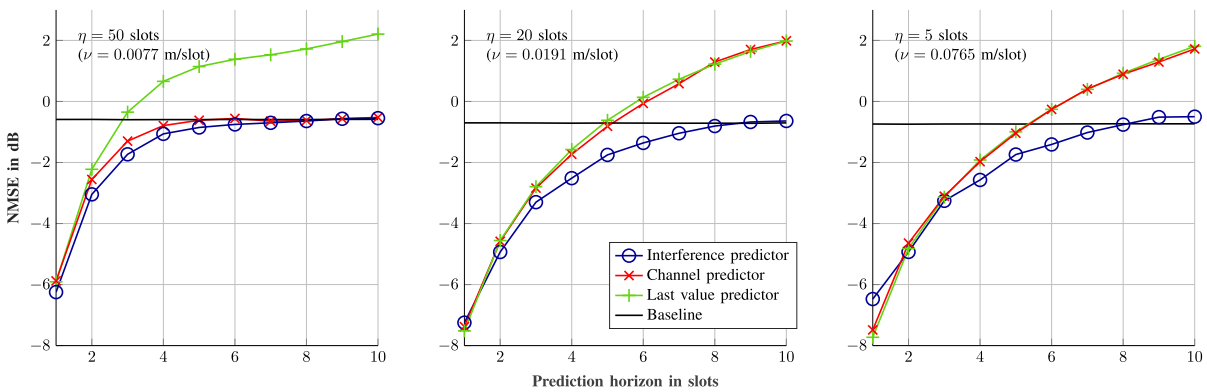

(a) Setup 1 (b) Setup 2 (c) Setup 3

Fig. 5. Predictor evaluation for increasing node mobility. Comparison between the proposed interference predictor (blue/o), a channel predictor that ignores the traffic influence (red/x), and a predictor that outputs as prediction its current observation (green/+). The interference coherence time for $\theta = 0.25$ is 5 time slots for subfigures a and b, and 3 time slots for subfigure c. The baseline of using the mean value of the interference as prediction is shown for reference.

Kalman predictor (dashed-dotted trace), for all p. The complexity savings from the steady-state formulation are more significant for shorter prediction horizons. For $p = 7$, the steady-state Kalman predictor requires 52% fewer operations for $\Delta = 5$ and 29% fewer for $\Delta = 10$. As the model order increases, the savings of the steady-state formulation slightly decrease for a given Δ. Both predictors show low implementation cost, with the steady-state version having the lowest in all cases. In summary, for implementation on highly constrained devices — like those employed in wireless sensor networks — the proposed steady-state predictor is convenient.

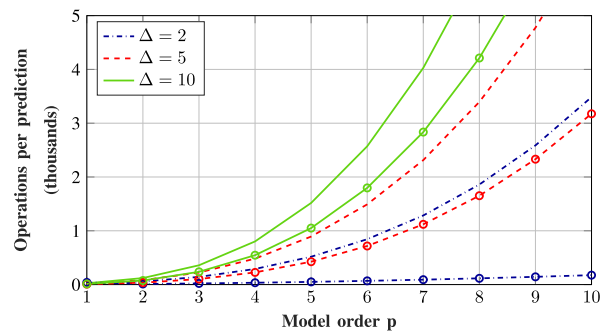

Fig. 6. Predictor complexity in terms of the number of floating point operations required per predicted sample. Results are shown for increasing model orders p with prediction horizons of $\Delta = 10$ (solid green), 5 (dashed red), and 2 (dash-dotted blue). Traces with (without) marker correspond to the steady-state (standard) Kalman filter predictor.

IV. Evaluation of Interference Prediction

The prediction performance is evaluated in terms of the normalized mean square error

$$\text{NMSE} = \frac{\sum_t (i(t+\Delta) - \hat{i}(t+\Delta))^2}{\sum_t i(t+\Delta)^2}, \tag{23}$$

which is a commonly used metric in channel prediction (see [32], [36], [37]), as the normalization with the squared power of the input signal allows to average realizations with different powers. Error results are always averaged over 10,000 network realizations with 1000 time slots interference sequences each.

A. Evaluation in the Base System

As a first step, the interference predictor is applied in the base system that was used for its parameterization: PPP, Rayleigh fading, and fixed message lengths. The setups from Table I are used with a node density of $\lambda = 0.01$ over an area of 10,000 square units, a path loss exponent $\alpha = 3$, and all nodes using unitary transmit power $\kappa = 1$.

Fig. 5 plots the NMSE over the prediction horizon in slots. Three predictors are compared: the interference predictor, a channel predictor, and a last value predictor. The channel predictor uses the same methodology as the interference predictor but with $\rho(\tau)$ accounting for the channel as the sole source of correlation ($\mu = 1$), and illustrates the impact of ignoring the traffic. The last value predictor simply takes its current interference observation as prediction. It is a performance reference for determining whether the extra (but low) complexity of the proposed predictor is justified. A "mean value predictor" serves as a baseline; it completely disregards interference dynamics and uses the mean value of the interference as prediction. As expected, the NMSE increases with an increasing prediction horizon for all three predictors in all setups. The interference predictor outperforms both the channel and last value predictors. Mobility increases from subplots (a) to (c) (i.e., Setups 1 to 3 from Table I). The channel predictor gets close to the interference predictor for the low mobility scenario (a). For higher node speeds, the channel predictor quickly degrades to the level of the last value predictor. The interference predictor crosses the baseline in all cases for a prediction horizon of eight slots. This horizon is significantly larger than the three and five slots obtained for the last value predictor (Subfigure (a) and Subfigures (b) and (c), respectively). This may justify its implementation cost.

Fig. 7 explores the predictors' behavior (adjusted for Setup 1 from Table I) as the message length changes: Longer messages result in more correlated interference and thus lower prediction

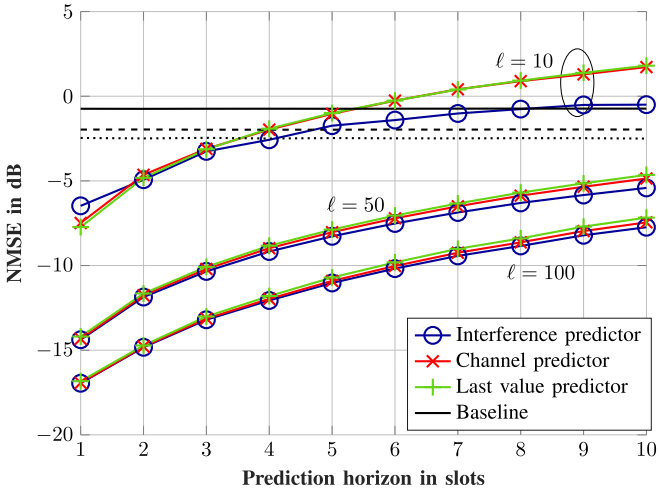

Fig. 7. Evaluation of the predictors for Setup 1 with different message lengths. The interference coherence time for $\theta = 0.25$ is 5, 21, and 47 slots for $\ell = 10$, 50, and 100, respectively. The mean value predictor baseline is shown for $\ell = 10$, 50, and 100.

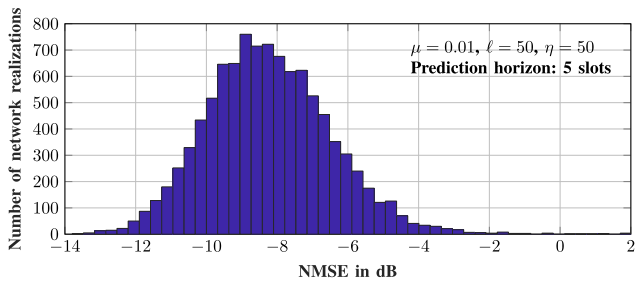

Fig. 8. NMSE distribution across network realizations. Results correspond to the case labeled $\ell = 50$ in Fig. 7 with a prediction horizon of five time slots.

error. In all cases, the interference predictor outperforms the others; however, the longer the messages, the more similar the predictors perform. For $\ell = 10$, the interference predictor attains horizons of eight slots with an error below the baseline, whereas the last value and channel predictors cross above the baseline for an horizon of five slots.

Recalling that the model used for prediction is independent of the individual realizations of the interference process, Fig. 8 explores how the prediction error deviates from its average value in Figs. 5 and 7 for different realizations of the network. Despite the fact that significant deviations exist for some realizations, most concentrate in the vicinity of the mean error.

B. Sensitivity to Other System Models

Now that we have seen that the interference predictor works well in the base system used for its design, it is of interest whether it also works in systems with other models. In other words, we are interested in how sensitive or robust the predictor is to variations or errors in the assumptions.

1) System Model: We evaluate the predictor in (22) for the following models: The node locations are no longer sampled from a homogeneous PPP but show some inhomogeneity.

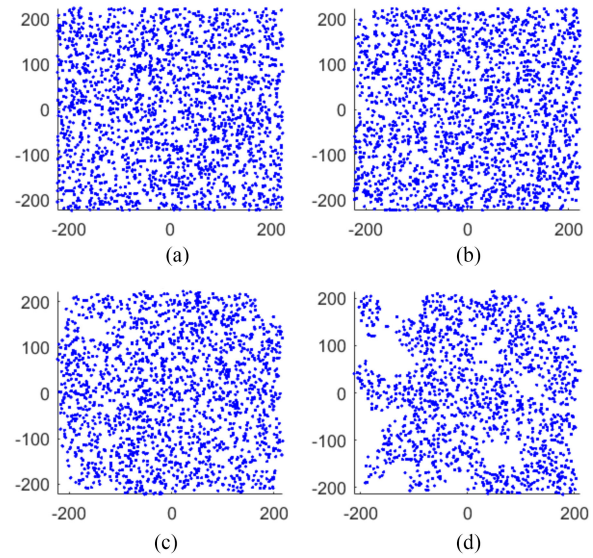

Fig. 9. Realizations of clustered node locations over an area of 200,000 square units. The original PPP (a) has an intensity $\lambda = 0.01$. The clustered nodes are generated by thinning this realization with distance parameter $r = 40$ and neighbor cardinality of (b) $k = 20$, (c) $k = 30$, and (d) $k = 40$.

The experienced small-scale fading is no longer Rayleigh but is rather Nakagami distributed. The message lengths are no longer fixed to ℓ but are sampled from a Poisson distribution with parameter ℓ. Nodes no longer transmit independently of the channel conditions but rather depend on the channel activity. The modeling of the locations is generalized by using an inhomogeneous random node distribution, in which nodes can be clustered in groups or concentrate at hotspots. This is achieved by thinning the original PPP realizations, such that nodes with at least a certain number k of neighboring nodes within a distance r are kept [38]. Some examples are shown in Fig. 9 with fixed r and increasing k. Changes to the node density resulting from this thinning do neither affect the interference correlation nor the predictor design, as (4) does not contain λ. The small-scale fading is generalized using the Nakagami distribution. Rayleigh fading, which was used for parameterization, corresponds to Nakagami fading with parameter $m = 1$, and we evaluate two larger m-values representing environments with fewer reflections. We apply a block fading channel model, where the channel states remain constant during the channel coherence time, and change to independent values afterward. Many wireless technologies implement channel sensing to minimize packet collisions [39], [40]. Therefore, it is relevant to investigate the impact of transmissions allowed only if the sensed channel activity is below a given threshold from the transmission power.

2) Performance Results: Fig. 10 shows the NMSE of the interference predictor for these setups if the interference samples at its input follow these alternative node placement, fading, and traffic models. Subfigure (a) shows the impact of the design mismatch in terms of the inhomogeneous node distribution. The predictor exhibits a robust behavior for significantly high inhomogeneity. Deviations are marginal and can only be appreciated for $k = 40$ (Fig. 9 (d)). Subfigure (b) assesses the impact of a

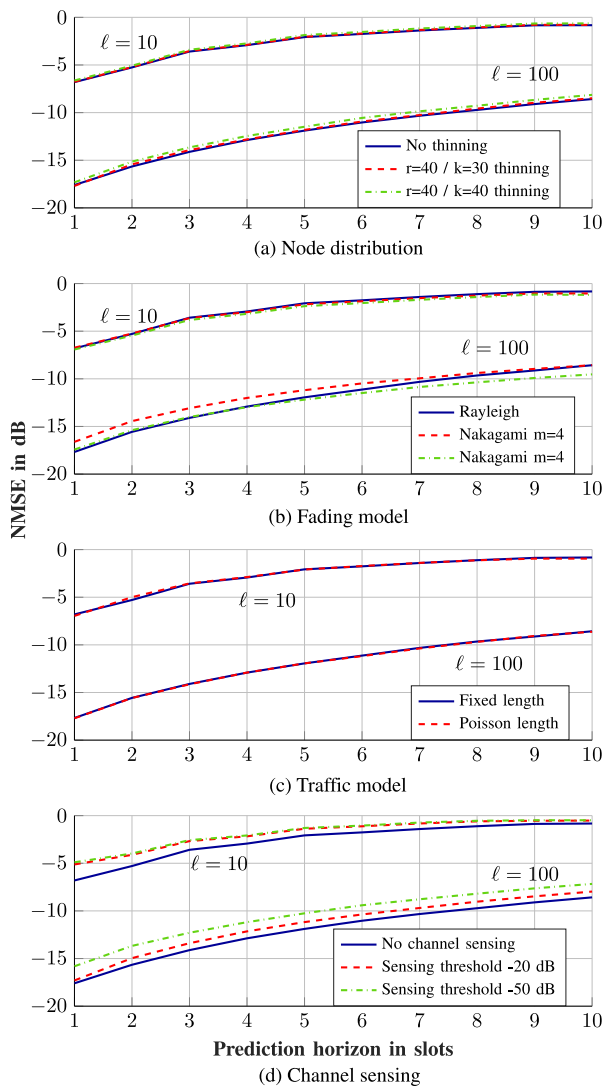

Fig. 10. Sensitivity of the predictor against (a) inhomogeneous node distribution (b) non-Rayleigh fading, (c) Poisson distributed message lengths, and (d) transmissions depending on channel activity. Results labeled $\ell = 10$ correspond to Setup 1 from Table I. Those labeled $\ell = 100$ extend the message length of that setup. The interference coherence time for $\theta = 0.25$ is 5 and 47 time slots for $\ell = 10$ and 100, respectively.

mismatch in the fading model, which the evaluation shows to be more significant for larger messages, although still close to the perfect match. Subfigure (c) reveals that the predictor is robust against the traffic model as long as the mean message length remains unchanged. The deviations are within the averaging noise. Nevertheless, Subfigure (d) indicates that the predictor is sensitive to mismatches in the channel access. Performance degrades as more intended transmissions are prevented to start (i.e., lower thresholds). The interference model should incorporate these mechanisms for best performance.

C. Evaluation for Specific Technologies

We now study the prediction performance for parameter values that are typical in two wireless technologies: Long Term Evolution (LTE) used for cellular systems [41] and IEEE 802.15.4 used for wireless sensor networks (WSN) [42]. This evaluation will highlight the versatility of the predictor. A message length of 20 slots is used in all scenarios.

TABLE III
SYSTEM PARAMETERS FOR LTE AND WSN SCENARIOS

Scenario	Speed ν	Traffic parameter μ	Channel coherence time η	Doppler shift Δ_f
LTE 1	6 km/h	0.01 / slot	225 slots	0.022
LTE 2	40 km/h	0.01 / slot	35 slots	0.148
LTE 3	80 km/h	0.01 / slot	17 slots	0.296
WSN	6 km/h	0.01 / slot	50 slots	0.125

The Δ_f is normalized to the system slot frequency.

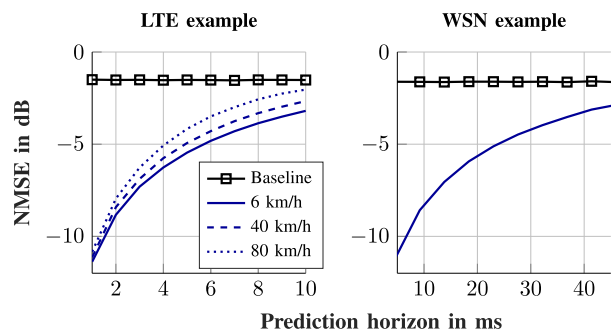

Fig. 11. Predictor performance for the different LTE and WSN scenarios from Table III. The interference coherence time for $\theta = 0.25$ is 10, 9, and 7 slots for speeds of 6, 40, and 80 km/h for LTE, and 9 slots for the WSN.

1) System Parameters: We consider an LTE downlink with carrier frequency f_c in the 2 GHz band. A base station assigns the mobile nodes to a specific subcarrier (or block of contiguous subcarriers). Scheduling decisions can be made every millisecond, defining a slot duration of one millisecond [41]. Each transmission experiences interference from the base stations of neighboring cells that are using the same frequency band (inter-cell interference). No exclusion area is modelled and hence interferers can be located arbitrarily close to the receiver. Although interferers are not mobile in this scenario, interference is impacted by node mobility leading to similar effects. In order to harness predictions at the base station, a prediction horizon above five slots is required to compensate for the processing delays involved [43]. We model the mobility with a maximum speed $\nu_{\max} = 1.67$ m/s $= 6$ km/h for pedestrians and 40 and 80 km/h for vehicles. We also consider a WSN with $f_c = 2.4$ GHz. The standard defines message lengths with a minimum of eight packets. With a packet duration of 577 μs, the slot duration is 4.6 ms [42]. These values give a prediction horizon of 23 ms for predicting five slots ahead. We use the same pedestrian mobility as in LTE. All parameters are summarized in Table III. The maximum Doppler shift is $\Delta_f = 2 f_c \nu_{\max}/c$ with the speed of light c.

2) Performance Results: Fig. 11 shows the ultimate predictor performance with these parameters if we map the prediction horizons to the signal timing and expected channel dynamics. We find that it is possible to predict beyond five slots with an error below the mean interference baseline in both cases. The

gains against the channel and the last value predictor are in line with those above.

D. Evaluation for Coexisting Technologies

A setup with multiple wireless technologies coexisting in the same band contributes to more efficient use of scarce resources (see [39], [40]). In this context, we explore how the proposed predictor is affected by interference from coexisting technologies not accounted for in its design. Specifically, we consider the coexistence of IEEE 802.11ax Wi-Fi and LTE in the 5 GHz band [40]. The predictor is designed for predicting the interference arising from the Wi-Fi deployment alone and its performance is affected by the interference generated by the LTE system operating in the same band.

1) System Parameters: Wi-Fi is operated in the single-user (SU) mode. Users and access points compete for a complete 20 MHz channel, following a simplified clear channel assessment (CCA) protocol. Channel access opportunities are arranged in 0.5 ms slots, at which users transmit with $\mu = 0.01$. Before initiating a transmission, the channel is sensed. If the sensed power is at least 50 dB (sensing threshold) below the transmit power, the channel is deemed idle and transmission begins. Otherwise, the transmission is discarded. The predictor design did not take such channel sensing into account.

The coexisting LTE system is considered in two modes: unlicensed spectrum (LTE-U) and licensed assisted access (LTE-LAA). In LTE-U, the base stations transmit without channel sensing. To mitigate their impact on the Wi-Fi, they adopt a discontinuous transmission pattern such that transmissions comply to a given duty-cycle (10% or 30% in our evaluation). In LTE-LAA, a fixed duty-cycle of 50% and the same threshold-based CCA as in Wi-Fi is used, where we consider levels of 100% and 50% of the Wi-Fi threshold.

The deployment of both systems follows the base system with an LTE base station density $\lambda = 0.001$, which is 10% of the Wi-Fi node density. The Wi-Fi nodes move at a pedestrian speed of 6 km/h; the LTE base stations are static. A transmission duration of 20 slots (10 ms) is used in both systems, which corresponds to LTE-LAA Class 4 access priority [40].

2) Performance Results: Fig. 12 shows the results for the coexistence setups, mapping the prediction horizons to the signal timing. Since the predictor design does not account for the CCA, the performance for Wi-Fi without CCA (design assumption) is shown for reference. Subfigure (a) shows the case of Wi-Fi and LTE-U coexistence. The CCA modifies the Wi-Fi interference dynamics, as can be seen from the degraded performance of Wi-Fi using CCA with respect to Wi-Fi without CCA (see also Fig. 10). The traces for Wi-Fi coexisting with LTE-U are below the trace for Wi-Fi using CCA alone, improving the predictor performance. This happens because the additional LTE-U interferers do not perform CCA and therefore make the aggregated interference dynamics closer to that for which the predictor is designed. For high duty-cycles, LTE-U increases the overall interference correlation making the predictor perform even better than for Wi-Fi without CCA. For the coexistence with LTE-LAA (Subfigure (b)), the impact of LTE on the predictor performance

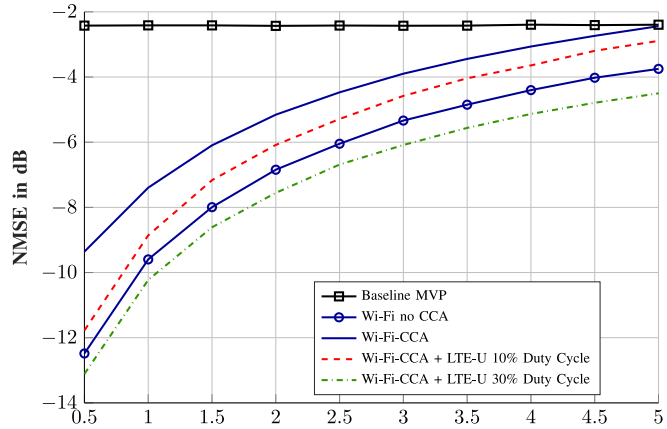

(a) Coexistence of Wi-Fi with LTE-U

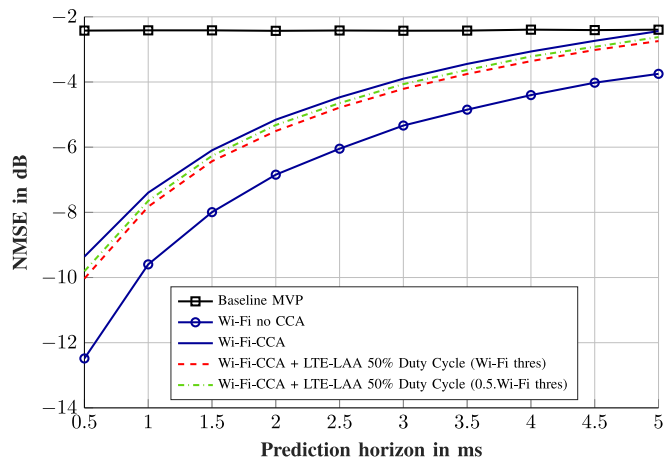

(b) Coexistence of Wi-Fi with LTE-LAA

Fig. 12. Predictor performance in a scenario with coexistence of Wi-Fi and LTE. The Wi-Fi interference coherence time for $\theta = 0.25$ is 5.3 ms for a 6 km/h node speed. Both technologies use a message length of 20 slots, equivalent to 10 ms.

is minimal.[1] Because LTE-LAA also uses a CCA mechanism, the dynamics of the overall interference is almost unchanged. Overall, we find that the predictor is robust to unknown interference of similar dynamics (LTE-LAA). Furthermore, the predictor sensitivity to the channel access method (CCA or not) is significant. The latter suggests that further models of channel access should be incorporated into the predictor design.

V. Conclusions and Outlook

This article showed how to harness the stochastic characterization of interference dynamics for the task of interference prediction in mobile networks. Our predictor designed as a recursive filter can be parameterized offline and shows reasonable computational complexity. Its performance analysis under matched and unmatched system conditions has

[1]Robustness against LTE interference does not necessarily imply fair coexistence between Wi-Fi and LTE-LAA. Prediction robustness in the context of this article indicates that the predictor is suitable for resource allocation applications, where it is used to find an optimal transmission slot [44].

demonstrated the prediction accuracy and robustness. Its versatility has been validated in multiple scenarios with parameters from LTE, sensor networks, and coexistence of Wi-Fi and LTE.

Future work will address additional theoretical and practical aspects of interference prediction. First, the use of nonlinear filters for deriving a higher accuracy predictor and the incorporation of alternative channel access schemes in the interference model should be addressed. Second, the predictor needs to be implemented and tested in programmable radios. Third, the impact of interference prediction on the network dynamics should be studied: in contrast to channel prediction, the use of interference prediction by multiple nodes changes the stochastic features of the interference process that is being predicted, and its feedback effect needs to be accounted for.

Appendix
Mapping $\rho(\tau)$ to an ARMA(p, q) Model

Starting from (6) and following [33, Ch. 17], we let τ take values from 0 to $p+q$ to generate the following equation set

$$\begin{bmatrix} \rho(0) & \cdots & \rho(p) \\ \rho(1) & \cdots & \rho(0) \\ \vdots & & \vdots \\ \rho(q) & \cdots & \rho(p-q) \\ \vdots & \ddots & \vdots \\ \rho(q+p) & \cdots & \rho(q) \end{bmatrix} \begin{bmatrix} a_0 \\ a_1 \\ \vdots \\ a_p \end{bmatrix} = \begin{bmatrix} b_0 & b_0 & \cdots & b_0 \\ 0 & b_0 & \cdots & b_0 \\ \vdots & \vdots & \ddots & \vdots \\ 0 & 0 & \cdots & b_0 \\ \vdots & \vdots & & \vdots \\ 0 & 0 & \cdots & 0 \end{bmatrix} \begin{bmatrix} b_0 \\ b_1 \\ \vdots \\ b_q \end{bmatrix}. \tag{24}$$

Specializing for $\tau = q+1, \ldots, q+p$ we have

$$\begin{bmatrix} \rho(q) & \cdots & \rho(q-p+1) \\ \rho(q+1) & \cdots & \rho(q-p) \\ \vdots & \ddots & \vdots \\ \rho(q+p) & \cdots & \rho(q) \end{bmatrix} \begin{bmatrix} a_1 \\ a_2 \\ \vdots \\ a_p \end{bmatrix} = -a_0 \begin{bmatrix} \rho(q+1) \\ \rho(q+2) \\ \vdots \\ \rho(q+p) \end{bmatrix}, \tag{25}$$

which imposing $a_0 = 1$ is recognized as the Yule Walker equations to solve for the AR coefficients $a_1, \ldots, a_p$ [34].

For determining the MA coefficients, consider (7) and (8) from introducing $\psi(t)$. All terms are known from the solution of (25). Thus, by running τ from 0 to q, we can generate the required set of equations to solve for $b_1, \ldots, b_q$ and σ_ϵ^2:

$$\begin{bmatrix} \psi(0) \\ \psi(1) \\ \vdots \\ \psi(q) \end{bmatrix} = \sigma_\epsilon^2 \begin{bmatrix} b_0 & b_1 & \cdots & b_{q-1} & b_q \\ b_1 & b_1 & \cdots & b_q & 0 \\ \vdots & \vdots & & \vdots & \vdots \\ b_q & 0 & \cdots & 0 & 0 \end{bmatrix} \begin{bmatrix} b_0 \\ b_1 \\ \vdots \\ b_q \end{bmatrix} \tag{26}$$

$$= \sigma_\epsilon^2 \begin{bmatrix} b_0 & b_1 & \cdots & b_{q-1} & b_q \\ 0 & b_0 & \cdots & b_{q-2} & b_{q-1} \\ \vdots & \vdots & & \vdots & \vdots \\ 0 & 0 & \cdots & 0 & b_0 \end{bmatrix} \begin{bmatrix} b_0 \\ b_1 \\ \vdots \\ b_q \end{bmatrix}, \tag{27}$$

which can be written as $\boldsymbol{\psi} = \sigma_\epsilon^2 \mathcal{M}^{\#} \mathbf{b} = \sigma_\epsilon^2 \mathcal{M} \mathbf{b}$, where $\boldsymbol{\psi}$ and $\mathbf{b}$ are the vector representations for $\psi(t)$ and the MA coefficients, respectively, and $\mathcal{M}^{\#}$ and $\mathcal{M}$ are the matrices in (26) and (27). The goal is to find the solution vector $\mathbf{b}$ for the nonlinear system $\boldsymbol{\psi} - \sigma_\epsilon^2 \mathcal{M}^{\#} \mathbf{b} = 0$, which is found iteratively. We use the procedure from Tunnicliffe-Wilson [45], where the rth approximation to the solution is computed from the $(r-1)$th instance as

$$\mathbf{b}_r = \mathbf{b}_{r-1} + \left\{ \sigma_\epsilon^2 \left(\mathcal{M}^{\#} + \mathcal{M} \right) \right\}_{r-1}^{-1} \left(\boldsymbol{\psi} - \sigma_\epsilon^2 \mathcal{M}^{\#} \mathbf{b} \right)_{r-1}.$$

As initialization we set $\sigma_\epsilon^2 = 1$ and $b_1 = b_2 = \cdots = b_q = 0$. Upon convergence we normalize to have $b_0 = 1$.

References

[1] G. Zheng, I. Krikidis, C. Masouros, S. Timotheou, D.-A. Toumpakaris, and Z. Ding, "Rethinking the role of interference in wireless networks," *IEEE Commun. Mag.*, vol. 52, no. 11, pp. 152–158, Nov. 2014.

[2] M. Haenggi, "Mean interference in hard-core wireless networks," *IEEE Commun. Lett.*, vol. 15, no. 8, pp. 792–794, Aug. 2011.

[3] U. Schilcher, S. Toumpis, M. Haenggi, A. Crismani, G. Brandner, and C. Bettstetter, "Interference functionals in Poisson networks," *IEEE Trans. Inf. Theory*, vol. 62, no. 1, pp. 370–383, Jan. 2016.

[4] Y. Yang and A. Petropulu, "Co-channel interference modeling and analysis in a Poisson field of interferers in wireless communications," *IEEE Trans. Signal Process.*, vol. 51, no. 1, pp. 64–76, Jan. 2003.

[5] E. S. Sousa and J. A. Silvester, "Optimum transmission ranges in a direct-sequence spread spectrum multihop packet radio network," *IEEE J. Sel. Areas Commun.*, vol. 8, no. 5, pp. 762–771, Jun. 1990.

[6] R. Mathar and J. Mattfeldt, "On the distribution of cumulated interference power in Rayleigh fading channels," *Wireless Netw.*, vol. 1, no. 1, pp. 31–36, 1995.

[7] M. Hellebrandt and R. Mathar, "Cumulated interference power and bit-error-rates in mobile packet radio," *Wireless Netw.*, vol. 3, no. 3, pp. 169–172, 1997.

[8] R. K. Ganti and M. Haenggi, "Interference and outage in clustered wireless ad hoc networks," *IEEE Trans. Inf. Theory*, vol. 55, no. 9, pp. 4067–4086, Sep. 2009.

[9] Y.-D. Yao and A. U. Sheikh, "Investigations into cochannel interference in microcellular mobile radio systems," *IEEE Trans. Veh. Technol.*, vol. 41, no. 2, pp. 114–123, May 1992.

[10] K. A. Hamdi, "On the statistics of signal-to-interference plus noise ratio in wireless communications," *IEEE Trans. Commun.*, vol. 57, no. 11, pp. 3199–3204, Nov. 2009.

[11] R. Ganti and M. Haenggi, "Spatial and temporal correlation of the interference in ALOHA ad hoc networks," *IEEE Commun. Lett.*, vol. 13, no. 9, pp. 631–633, Sep. 2009.

[12] U. Schilcher, C. Bettstetter, and G. Brandner, "Temporal correlation of interference in wireless networks with Rayleigh fading," *IEEE Trans. Mobile Comput.*, vol. 11, no. 12, pp. 2109–2120, Dec. 2012.

[13] M. Haenggi and R. Smarandache, "Diversity polynomials for the analysis of temporal correlations in wireless networks," *IEEE Trans. Wireless Commun.*, vol. 12, no. 11, pp. 5940–5951, Nov. 2013.

[14] R. Tanbourgi, H. S. Dhillon, J. G. Andrews, and F. K. Jondral, "Effect of spatial interference correlation on the performance of maximum ratio combining," *IEEE Trans. Wireless Commun.*, vol. 13, no. 6, pp. 3307–3316, Jun. 2014.

[15] R. Tanbourgi, "Diversity combining under interference correlation in wireless networks," Ph.D. dissertation, Karlsruhe Inst. of Technol., Karlsruhe, Germany, Jun. 2015.

[16] K. Koufos and C. P. Dettmann, "Temporal correlation of interference and outage in mobile networks over one-dimensional finite regions," *IEEE Trans. Mobile Comput.*, vol. 17, no. 2, pp. 475–487, Feb. 2018.

[17] U. Schilcher, J. F. Schmidt, M. K. Atiq, and C. Bettstetter, "Autocorrelation and coherence time of interference in Poisson networks," *IEEE Trans. Mobile Comput.*, vol. 19, no. 7, pp. 1506–1518, Jul. 2020.

[18] M. Haenggi, "Diversity loss due to interference correlation," *IEEE Commun. Lett.*, vol. 16, no. 10, pp. 1600–1603, Oct. 2012.

[19] R. Tanbourgi, H. S. Dhillon, J. G. Andrews, and F. K. Jondral, "Dual-branch MRC receivers under spatial interference correlation and Nakagami fading," *IEEE Trans. Commun.*, vol. 62, no. 6, pp. 1830–1844, Jun. 2014.

[20] M. K. Atiq, U. Schilcher, J. F. Schmidt, and C. Bettstetter, "Semi-blind interference prediction in wireless networks," in *Proc. ACM Intern. Conf. Model., Anal. Simul. Wireless Mobile Syst.*, Miami Beach, FL, USA, Nov. 2017, pp. 19–23.

[21] Y. Cong, X. Zhou, and R. A. Kennedy, "Interference prediction in mobile ad hoc networks with a general mobility model," *IEEE Trans. Wireless Commun.*, vol. 14, no. 8, pp. 4277–4290, Aug. 2015.
[22] Z. Gong and M. Haenggi, "Interference and outage in mobile random networks: Expectation, distribution, and correlation," *IEEE Trans. Mobile Comput.*, vol. 13, no. 2, pp. 337–349, Feb. 2014.
[23] X. Lin, J. Andrews, and A. Ghosh, "Spectrum sharing for device-to-device communication in cellular networks," *IEEE Trans. Wireless Commun.*, vol. 13, no. 12, pp. 6727–6740, Dec. 2014.
[24] H. ElSawy, E. Hossain, and M.-S. Alouini, "Analytical modeling of mode selection and power control for underlay D2D communication in cellular networks," *IEEE Trans. Commun.*, vol. 62, no. 11, pp. 4147–4161, Nov. 2014.
[25] N. Lee, X. Lin, J. Andrews, and R. Heath, "Power control for D2D underlaid cellular networks: Modeling, algorithms, and analysis," *IEEE J. Sel. Areas Commun.*, vol. 33, no. 1, pp. 1–13, Jan. 2015.
[26] M. Erturk, S. Mukherjee, H. Ishii, and H. Arslan, "Distributions of transmit power and SINR in device-to-device networks," *IEEE Commun. Lett.*, vol. 17, no. 2, pp. 273–276, Feb. 2013.
[27] Q. Ye, M. Al-Shalash, C. Caramanis, and J. Andrews, "Resource optimization in device-to-device cellular systems using time-frequency hopping," *IEEE Trans. Wireless Commun.*, vol. 13, no. 10, pp. 5467–5480, Oct. 2014.
[28] J. F. Schmidt, M. K. Atiq, U. Schilcher, and C. Bettstetter, "Underlay device-to-device communications in LTE-A: Uplink or downlink?," in *Proc. IEEE Int. Symp. Personal, Indoor, Mobile Radio Commun.*, Hong Kong, China, Sep. 2015, pp. 1542–1546.
[29] W. Jakes, *Microwave Mobile Communications*. New York, NY, USA: Wiley, 1974.
[30] D. Stoyan, W. S. Kendall, and J. Mecke, *Stochastic Geometry and Its Applications*, 2nd ed. Chichester, U.K.: Wiley, 1995.
[31] M. Haenggi and R. Ganti, "Interference in Large Wireless Networks," Foundations and Trends® in Networking, vol. 3, no. 2, pp. 127–248.
[32] A. Duel-Hallen, "Fading channel prediction for mobile radio adaptive transmission systems," *Proc. IEEE*, vol. 95, no. 12, pp. 2299–2313, Dec. 2007.
[33] D. S. G. Pollock, *Time Series Analysis Signal Processing and Dynamics*. London, U.K.: Academic, 1998.
[34] P. A. Regalia, *Adaptive IIR Filtering in Signal Processing and Control*. New York, NY, USA: Marcel Dekker, Inc., 1995.
[35] C. Chui and G. Chen, *Kalman Filtering - With Real-Time Applications*. 2nd ed. Berlin, Germany: Springer-Verlag, 1991.
[36] J. F. Schmidt, J. E. Cousseau, R. Wichman, and S. Werner, "Low-complexity channel prediction using approximated recursive DCT," *IEEE Trans. Circuits Syst. I: Reg. Papers*, vol. 58, no. 10, pp. 2520–2530, Oct. 2011.
[37] R. O. Adeogun, "Channel prediction for mobile MIMO wireless communiction systems," Ph.D. dissertation, Victoria Univ. of Wellington, 2015.
[38] C. Bettstetter, M. Gyarmati, and U. Schilcher, "An inhomogeneous node distribution and its stochastic properties," in *Proc. ACM/IEEE Intern. Symp. Model., Anal., Simul. Wireless Mobile Syst.*, Chania, Greece, Oct. 2007, pp. 400–404.
[39] V. Sathya, S. M. Kala, M. I. Rochman, M. Ghosh, and S. Roy, "Standardization advances for cellular and Wi-Fi coexistence in the unlicensed 5 and 6 GHz bands," *GetMobile: Mobile Comp. Comm.*, vol. 24, no. 1, p. 5–15, Aug. 2020.
[40] M. Mehrnoush, V. Sathya, S. Roy, and M. Ghosh, "Analytical modeling of Wi-Fi and LTE-LAA coexistence: Throughput and impact of energy detection threshold," *IEEE/ACM Trans. Netw.*, vol. 26, no. 4, pp. 1990–2003, Aug. 2018.
[41] 3GPP TS 36.213, "Evolved universal terrestrial radio access: Physical layer procedures (Release 14)," Apr 2017.
[42] IEEE Std 802.15.4, "Wireless medium access control and physical layer specifications for low rate wireless personal area networks," Sep. 2006.
[43] J. F. Schmidt, J. E. Cousseau, R. Wichman, and S. Werner, "Bit loading using imperfect CSIT for prediction-based resource allocation in mobile OFDMA," *IEEE Trans. Veh. Technol.*, vol. 60, no. 8, pp. 4082–4088, Oct. 2011.
[44] J. F. Schmidt, J. E. Cousseau, R. Wichman, and S. Werner, "Prediction based resource allocation in OFDMA," in *Proc. IEEE Conf. Inf. Sci. Syst. (CISS)*, Baltimore, USA, Mar. 2011.
[45] G. Wilson, "Factorization of the covariance generating function of a pure moving average process," *SIAM J. Numer. Anal*, vol. 6, no. 1, pp. 1–7, 1969.

Jorge F. Schmidt received B.Sc. and D.Sc. degrees in electrical engineering from the Universidad Nacional del Sur, Argentina, in 2005 and 2011, respectively. From 2012 to 2014, he was with the University of Vigo, Spain. In 2014, he joined the Institute of Networked and Embedded Systems, University of Klagenfurt, Austria. Since 2016, he has also been a Senior Researcher with Lakeside Labs GmbH, Austria. His research interests are in interference modeling and management in wireless systems. He was the recipient of the Best Paper Award from the ACM SIGSIM.

Udo Schilcher received Dipl.-Ing. degrees in applied informatics and in mathematics, in 2005 and 2006, respectively, and the Dr. techn. degree in wireless communications in 2011, all with distinction from the University of Klagenfurt. Since 2011, he has held senior positions with the Institute of Networked and Embedded Systems, University of Klagenfurt, and with Lakeside Labs GmbH. His main interests are interference dynamics in wireless networks and stochastic geometry. He was awarded the Best Paper Award from the IEEE Vehicular Technology Society.

Mahin K. Atiq received her master's degree in information and communication engineering from Sejong University, Seoul, South Korea, in 2014. She is currently working toward the doctoral degree in interference in wireless networks. From 2015 to 2019, she was a Research and Teaching Staff Member with the University of Klagenfurt. She is currently a Scientist with Silicon Austria Labs GmbH, Austria. Her research interests include wireless communication and stochastic modeling.

Christian Bettstetter (Senior Member, IEEE) received the Dr.-Ing. degree (*summa cum laude*) in electrical and information engineering from TU München, Munich, Germany, in 2004. He is currently a Professor and the Head of the Institute of Networked and Embedded Systems, University of Klagenfurt, Austria, and the Scientific Director of Lakeside Labs GMBH, Austria. His research interests are in wireless connectivity and self-organization of networked systems with application to telecommunications and robotics.